Electronic Supplementary Material (ESI) for Nanoscale Advances.

Supplementary Information

Doping-free bandgap tunability in the Fe_2O_3 nanostructured films

Sujit A. Kadam,[a] Giang Thi Phan[a], Duy Van Pham,*[,a] Ranjit A. Patil,[a] Chien-Chih Lai,[a] Yan-Ruei Chen,[b] Yung Liou,[b] and Yuan-Ron Ma*[,a]

[a] *Department of Physics, National Dong Hwa University, Hualien 97401, Taiwan*

[b] *Institute of Physics, Academia Sinica, Taipei 11529, Taiwan*

*Corresponding author:

E-mail: ronma@mail.ndhu.edu.tw

E-mail: duypham0611@gmail.com

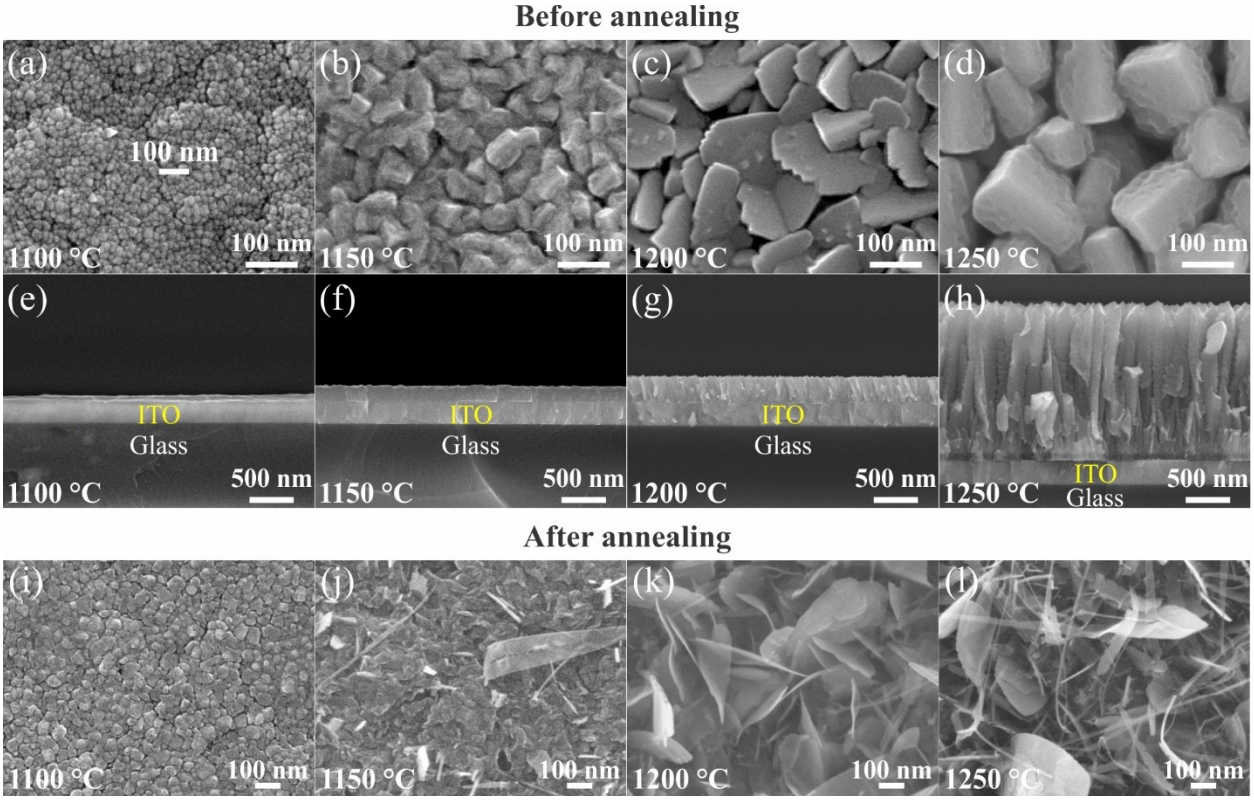

Figure S1. Surface morphology. (a)-(h) FESEM images showing the top view and side view of the FeO_x nanostructures synthesized at 1100, 1150, 1200, and 1250 °C. (i)-(l) FESEM images showing top-views of Fe_2O_3 nanostructured films after annealing at 500 °C for 4 hours in ~500 Torr O_2 atmosphere.

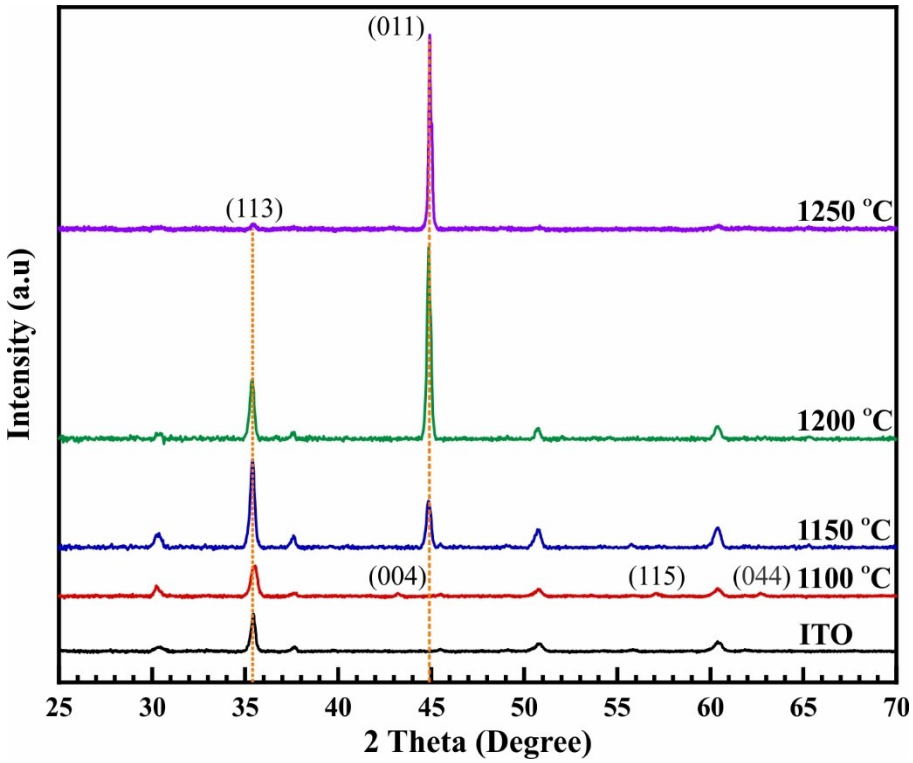

Figure S2. Determination of the crystal structure. XRD patterns of the samples synthesized at temperatures of 1100, 1150, 1200, and 1250 °C before annealing. The XRD peaks of the sample synthesized at 1100 °C are indexed with the cubic structure of Fe_3O_4, which is in the space group of F d -3 m with lattice constants of a = b = c = 8.399 nm, $\alpha = \beta = \gamma = 90^0$ (ICSD 77590). While the XRD peaks of the samples synthesized at 1150, 1200, and 1250 °C are attributed to the cubic structure of metallic iron with the space group of F m -3 m and lattice constants of a = b = c = 4.341 nm, $\alpha = \beta = \gamma = 90^0$ (ICSD 27856).

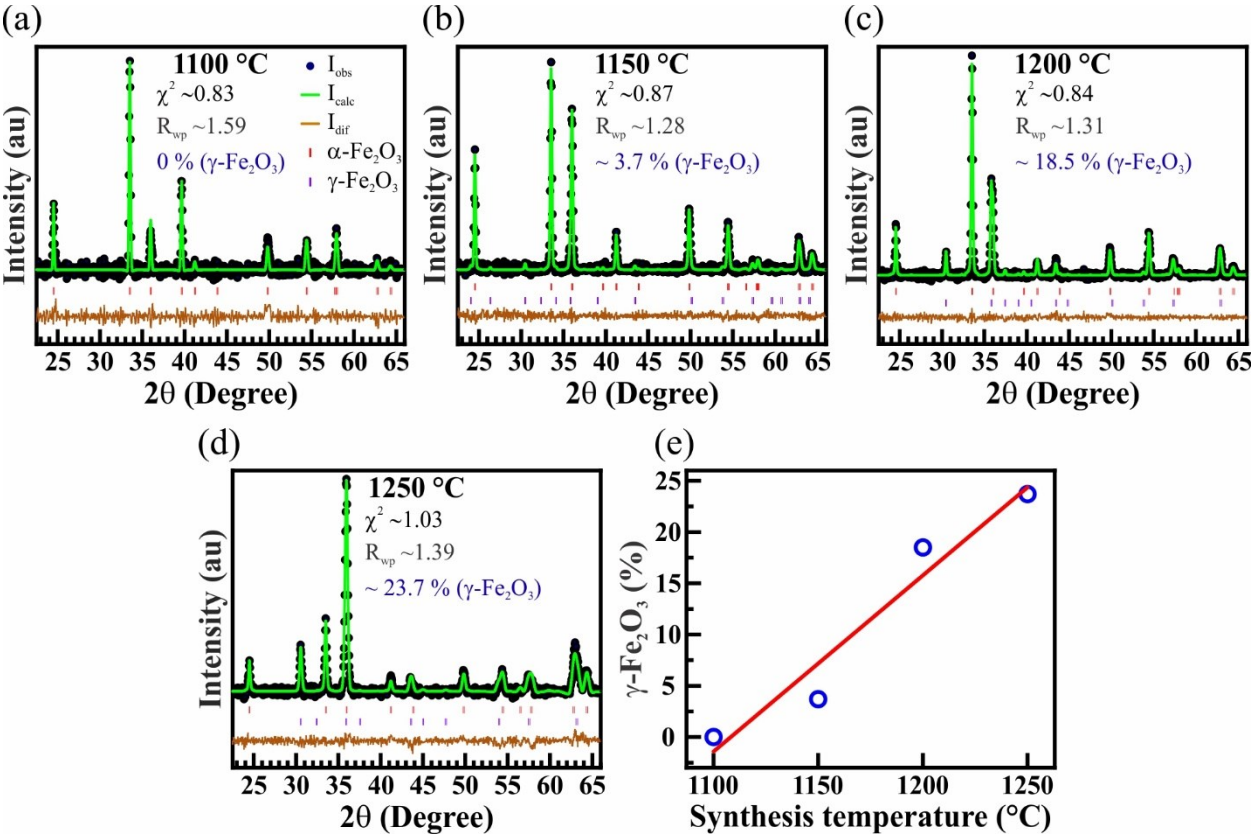

Figure S3. Rietveld-refined XRD pattern (a)-(d) Reitveld refinement patterns of the Fe_2O_3 nanostructured films@1100, 1150, 1200, and 1250 °C on fused quartz substrates. (e) Linear graph showing the linear increase of the γ-Fe_2O_3 from 0 to 23.7 % with the elevation of the synthesis temperature.

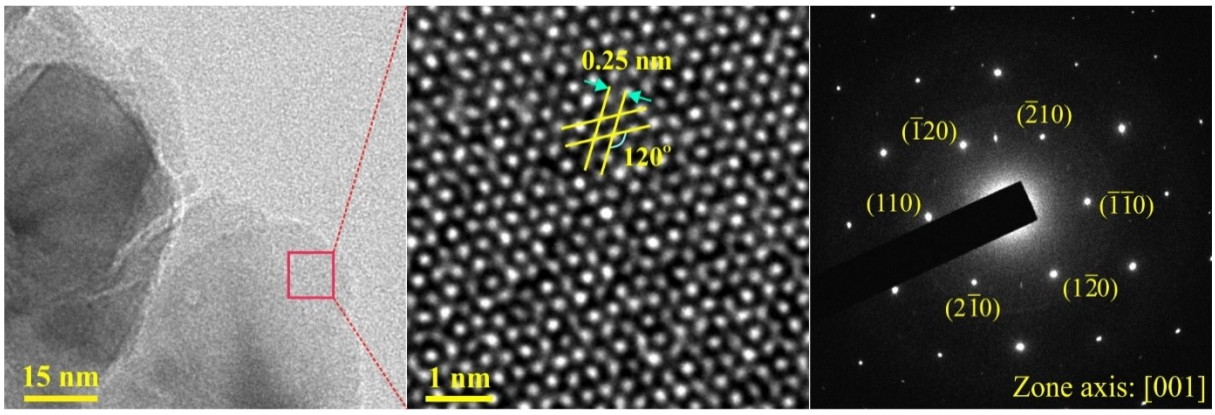

Figure S4. Crystal structure determination of the Fe_2O_3 thin film@1100 °C. Low-, High-resolution TEM images and SAED pattern of the Fe_2O_3 thin film@1100 °C. TEM results confirm that the Fe_2O_3 thin film@1100 °C contains only the trigonal (α) phase.

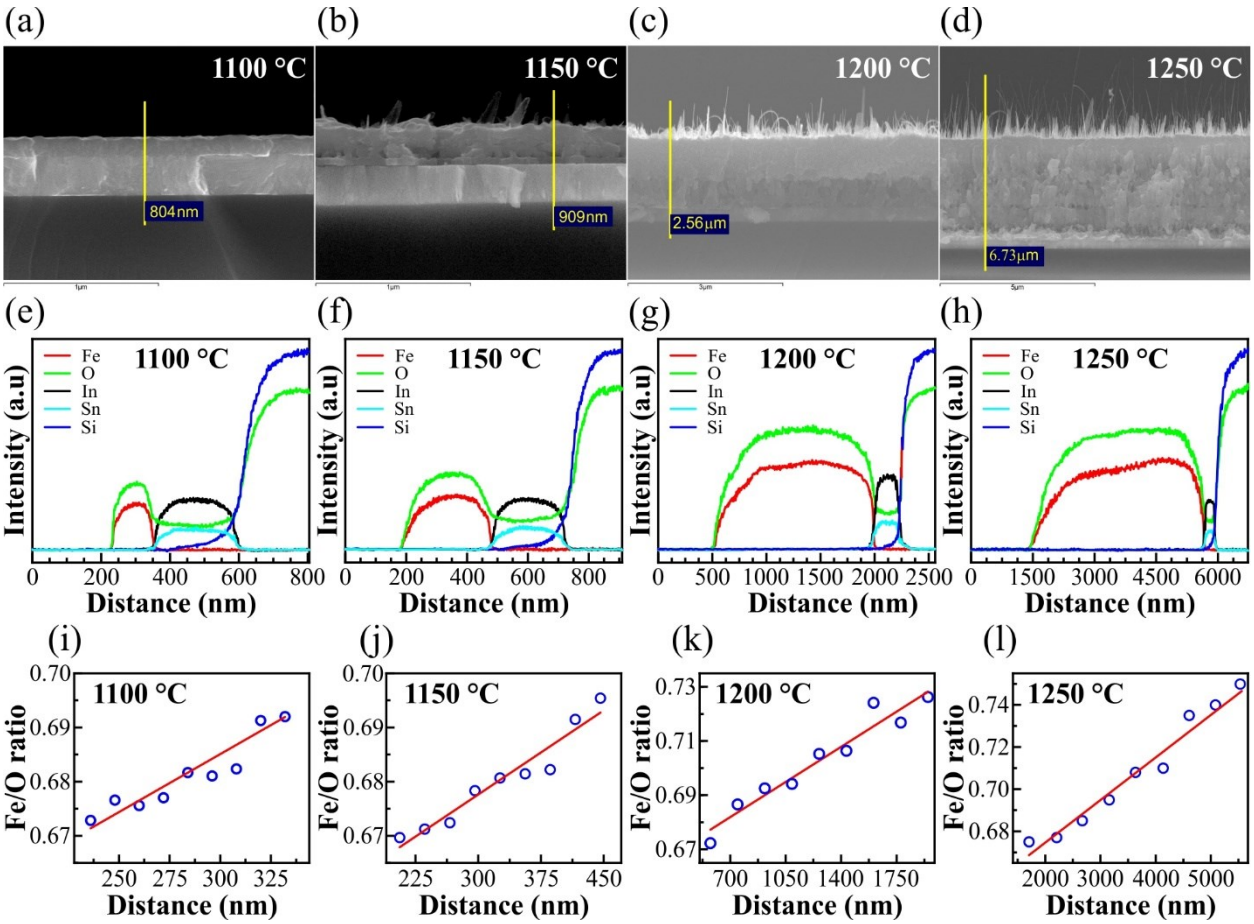

Figure S5. EDS line profile. (a)-(d) SEM images with the yellow line across the Fe_2O_3 nanostructured films synthesized at various temperatures of 1100, 1150, 1200, and 1250 °C. (e)-(h) EDS intensity profiles of Fe, O, In, Sn, and Si. (i)-(l) Fe/O ratio at various distances on the Fe_2O_3 nanostructured films.

In order to further understand the compositional change of Fe and O in the Fe_2O_3 nanostructured films, the EDS line profile was used to investigate. The EDS intensities of each element have been detected along the yellow line that runs across the thickness of the Fe_2O_3 nanostructured films, as shown in Fig. S5a-d. EDS intensity profiles of Fe, O, In, Sn, and Si as functions of distance are displayed in Fig. S5e-h. It can be seen that the EDS line profiles for all the Fe_2O_3 nanostructured films are similar. The Fe/O ratio calculated using the EDS intensity profiles at various distances on the Fe_2O_3 nanostructured films is shown in Fig. S5i-l. Obviously, the Fe/O ratio increases linearly with increasing distance, or in other words the Fe/O ratio becomes higher the closer the interface is between Fe_2O_3 film and ITO substrate. However, the increase in the Fe/O ratio in the

Fe_2O_3 nanostructured films@1100 and 1150 ^oC is negligible, while this in the Fe_2O_3 nanostructured films@1200 and 1250 ^oC is much higher. This is due to the large thickness of Fe_2O_3 film@1200 and 1250 ^oC, which reduces the diffusion of oxygen into the Fe_2O_3 film during annealing at 500 ^oC. The increase in the Fe/O ratio in the Fe_2O_3 nanostructured films also creates structural disorder, leading to the reduction in the bandgap of the Fe_2O_3 nanostructured films.

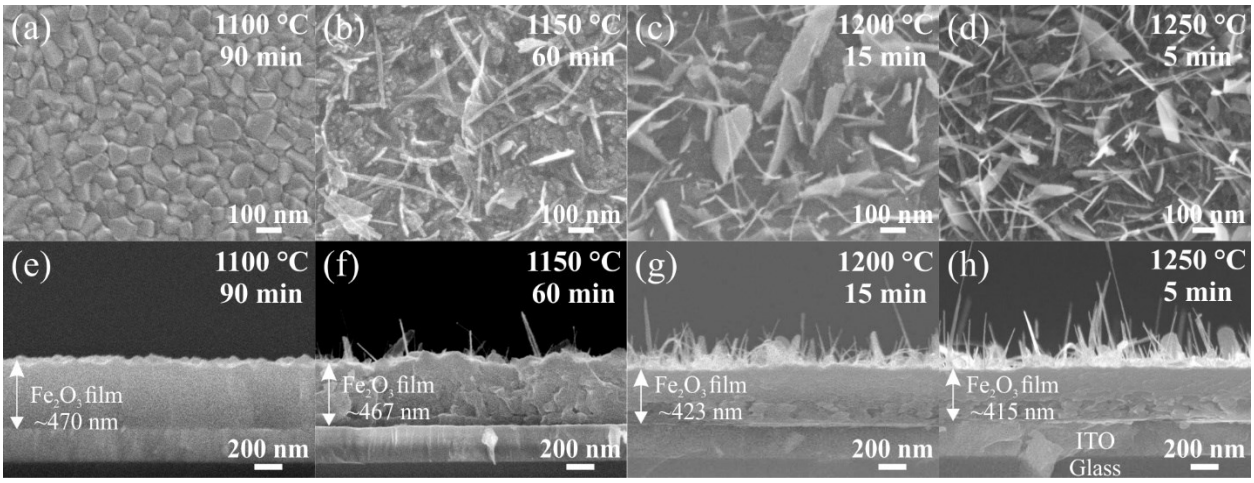

Figure S6 Surface morphology of the Fe_2O_3 nanostructured films with similar thickness. (a)-(h) FESEM images showing the top view and side view of the Fe_2O_3 nanostructured films synthesized at various synthesis parameters of (1100 ^oC, 90 min), (1150 ^oC, 60 min), (1200 ^oC, 15 min), and (1250 ^oC, 5 min)

To obtain the films of nearly similar thickness. The Fe_2O_3 nanostructured films were synthesized on ITO/glass substrates using the HFMOVD technique at various synthesis parameters of (1100 ^oC, 90 min), (1150 ^oC, 60 min), (1200 ^oC, 15 min), and (1250 ^oC, 5 min). The FESEM images in Fig. S6 show the top and side views of the large-area arrays of the Fe_2O_3 nanostructured films synthesized at the various synthesis parameters. Clearly, the morphology of all samples in this synthesis condition is the same as before (Fig. 2 and Fig. S1), except for the thickness of the Fe_2O_3 nanostructured films.

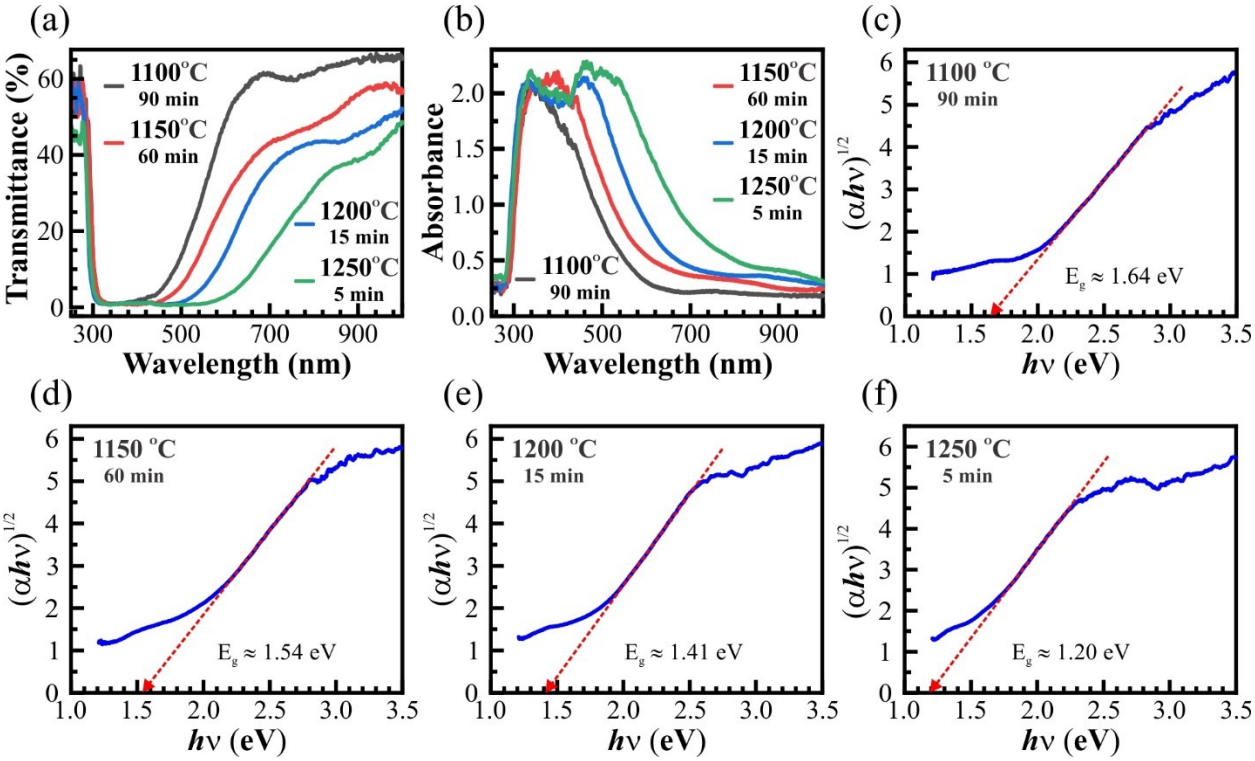

Figure S7 Bandgap properties of the Fe_2O_3 nanostructured films with similar thickness. (a) The transmittance and (b) absorbance spectra of the Fe_2O_3 nanostructured films synthesized at various synthesis parameters. (c)-(f) The linear graphs of $(\alpha h\nu)^{1/2}$ *vs.* hν for determining the E_g of the Fe_2O_3 nanostructured films with similar thickness.

The bandgap of the Fe_2O_3 nanostructured films with similar thickness has been also investigated using optical spectroscopy. Fig. S7 shows the transmittance, absorbance spectra, and the indirect bandgap calculation of the Fe_2O_3 nanostructured films with similar thickness. It is clear that the bandgap also reduces with the elevated synthesis temperatures. The bandgap reduction of 0.44 eV is just 0.11 eV small than that of 0.55 eV of the Fe_2O_3 nanostructured films with different thicknesses, as shown in Fig. 5. The energy difference of 0.11 eV can be attributed to the effect of thickness on the bandgap of the Fe_2O_3 film nanofiber. Obviously, the bandgap reduction is strongly governed by the crystal composition of the cubic (γ) phase and the amount of the Fe^{2+} cations in the Fe_2O_3 nanostructured films.

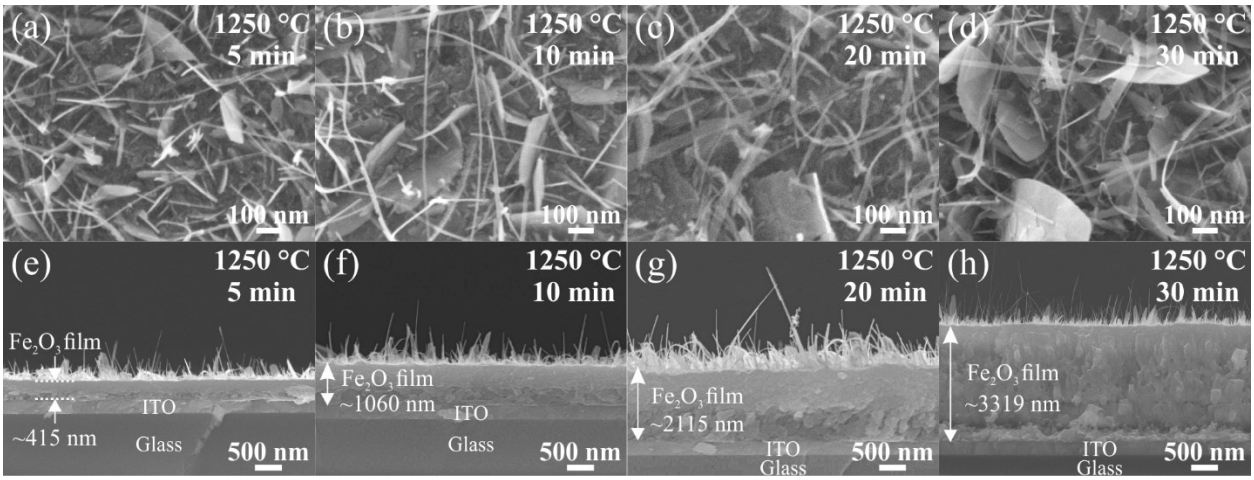

Figure S8. Surface morphology of the Fe_2O_3 nanostructured films at various deposition time. (a)-(h) FESEM images showing the top view and side view of the Fe_2O_3 nanostructured films synthesized at a synthesis temperature of 1250 ^oC for 5, 10, 20, and 30 min.

In order to further understand the effect of thickness on the bandgap of the Fe_2O_3 nanostructured films. The Fe_2O_3 nanostructured films were synthesized on ITO/glass substrates using the HFMOVD technique at a synthesis temperature of 1250 ^oC for 5, 10, 20, and 30 min. The FESEM images in Fig. S8 show the top and side views of the large-area arrays of the Fe_2O_3 nanostructured films synthesized at various deposition times. Nanofibers and nanosheets with similar dimensions are formed on all samples, while the average thickness of the Fe_2O_3 buffer layers increases from ~ 415 to ~3319 nm with the increase of the deposition time.

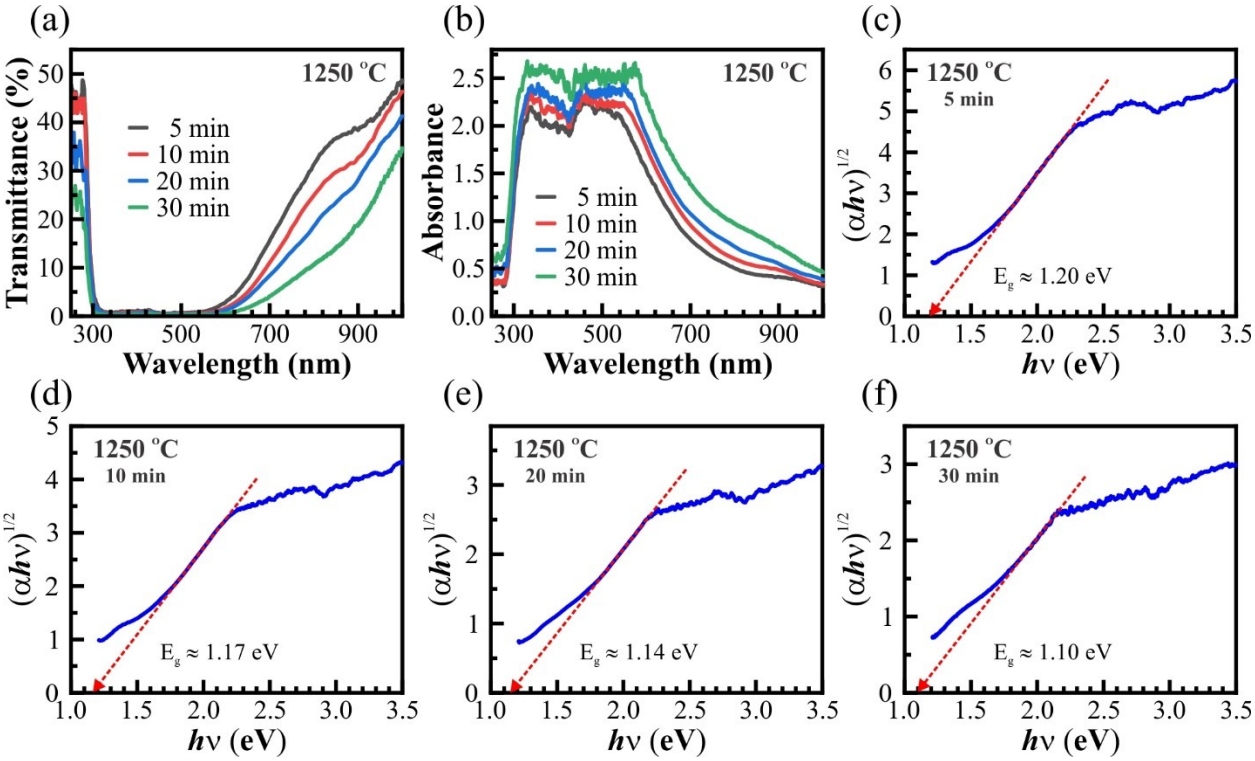

Figure S9. Bandgap properties of the Fe_2O_3 nanostructured films at various deposition time. (a) The transmittance and (b) absorbance spectra of the Fe_2O_3 nanostructured films synthesized at a synthesis temperature of 1250 °C for 5, 10, 20, and 30 min. (c)-(f) The linear graphs of $(\alpha h\nu)^{1/2}$ *vs.* hν for determining the E_g of the Fe_2O_3 nanostructured films at various deposition time.

The optical spectroscopy was also used to discuss the effect of thickness on the bandgap of the Fe_2O_3 nanostructured films. The transmittance, absorbance spectra, and the indirect bandgap calculation are shown in Fig. S9. The bandgap of the Fe_2O_3 nanostructured films synthesized at 1250 °C for 5, 10, 20, and 30 min are 1.20, 1.17, 1.14, and 1.10 eV, respectively. The bandgap reduction of 0.1 eV is well consistent with the results that discussed above. Therefore, the effect of thickness does not play a significant role in the bandgap reduction of Fe_2O_3 nanostructured films.

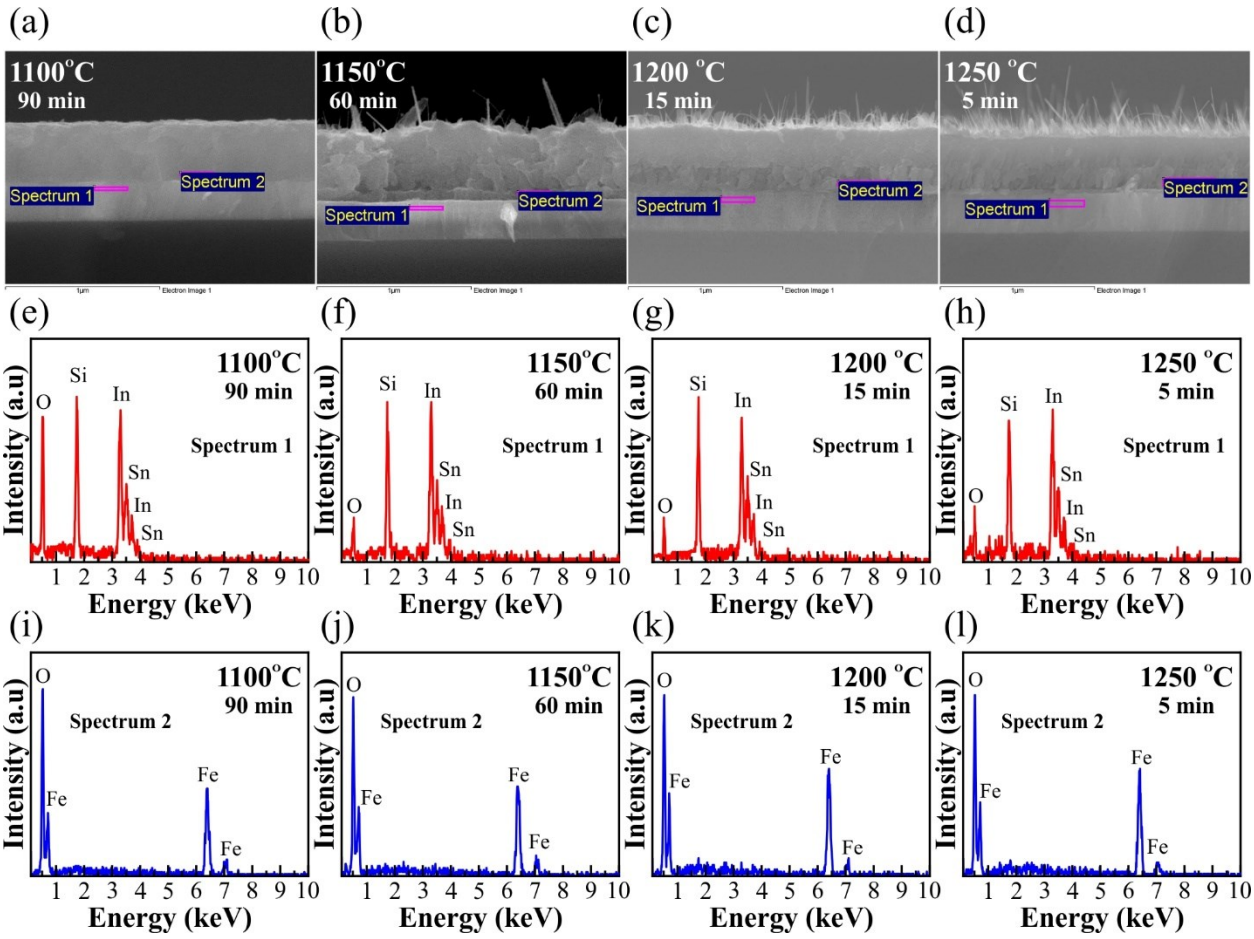

Figure S10. EDS spectra of the Fe_2O_3 nanostructured films. (a)-(d) EDS images of the Fe_2O_3 nanostructured films synthesized at various synthesis parameters. (e)-(f) EDS spectra are measured on the ITO layer. The EDS peak of Fe does not appear in these EDS spectra. (i)-(l) EDS spectra are measured on the Fe_2O_3 buffer layer. No EDS peaks of In and Sn are observed in these EDS spectra

During annealing the samples at 500 °C. Fe may diffuse into ITO substrate. Similarly, Sn and In from ITO substrates may mix with the iron oxide through the interface between the Fe_2O_3 buffer layer and the ITO substrate. However, the diffusion of Fe into ITO substrate and the mixing of Sn and In with the iron oxide is negligible. Fig. S10 shown the EDS spectra of the F_2O_3 nanostructured films. The EDS spectra were measured very close to the interface between the Fe_2O_3 buffer layer and the ITO substrate. Evidently, the EDS peak of Fe does not appear in the EDS spectra, which measured at the ITO substrates. Similarly, no EDS peaks of In and Sn are observed in the EDS spectra, which measured at the Fe_2O_3 buffer layer. In addition, the absorbance and transmittance

spectra of the F_2O_3 nanostructured films have been recorded using ITO substrate as a reference. The optical absorption of the ITO substrate has been removed during the optical measurement. Therefore, the ITO substrate only affects the morphology of the Fe_2O_3 buffer layer but does not affect the bandgap tunability in the Fe_2O_3 nanostructured films.

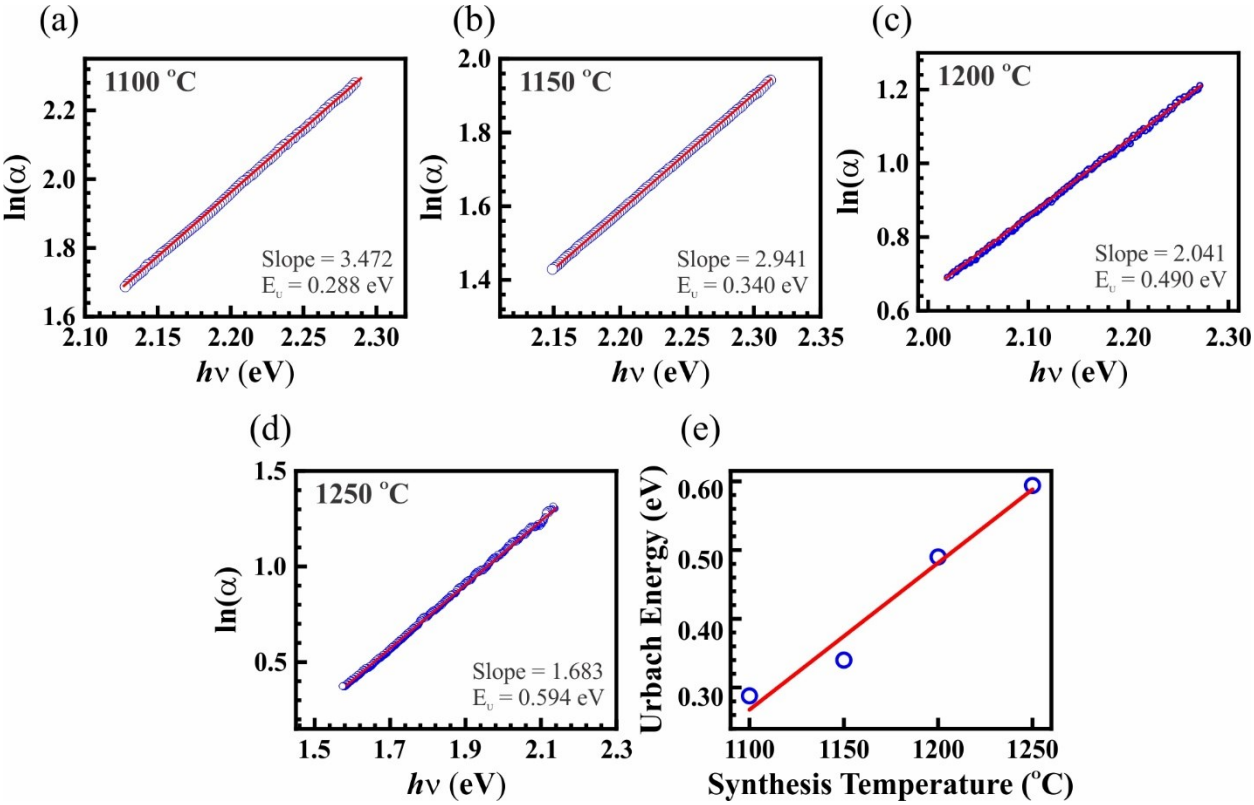

Figure S11. Urbach energy (E_u). (a)-(d) the graphs of ln(α) versus $h\nu$ for the Fe_2O_3 nanostructured films@1100, 1150, 1200, and 1250 °C. The E_u is determined by the reciprocal slope of the linear fit. (e) The linear graphs show the increase of the E_u with the elevated synthesis temperatures.

The phase combination and cation mixture create the structural disorder, which leads to the formation of the localized states. To determine the structural disorder of the Fe_2O_3 nanostructured films, the Urbach energy (E_u) has been used to investigate. The E_u is calculated using the equation (1).

$$\alpha = \alpha_0 exp\left(\frac{h\nu}{E_u}\right) \quad (1)$$

where α is the absorption coefficient, α_0 is a constant, $h\nu$ is the photon energy and E_u is the Urbach energy. Fig. S11a-d shows the graphs of ln(α) versus $h\nu$ for the Fe_2O_3 nanostructured films@1100, 1150, 1200, and 1250 °C. The E_u is determined by the reciprocal slope of the linear fit. The values of the E_u are 0.288, 0.340, 0.490, and 0.594 eV for the Fe_2O_3 nanostructured films@1100, 1150, 1200, and 1250 °C, respectively. The linear graph in Fig. S11e shows the E_u of the Fe_2O_3

nanostructured films@1100, 1150, 1200, and 1250 ^{o}C versus temperature. Obviously, the E_u increases linearly with elevated synthesis temperature. The linear increase of the E_u is due to the linear increase of crystal composition of the cubic (γ) phase and the amount of the Fe^{2+} cations with the elevated synthesis temperature. The increase of the E_u indicates the increase of localized states, which leads to a significant bandgap reduction of the Fe_2O_3 nanostructured films.

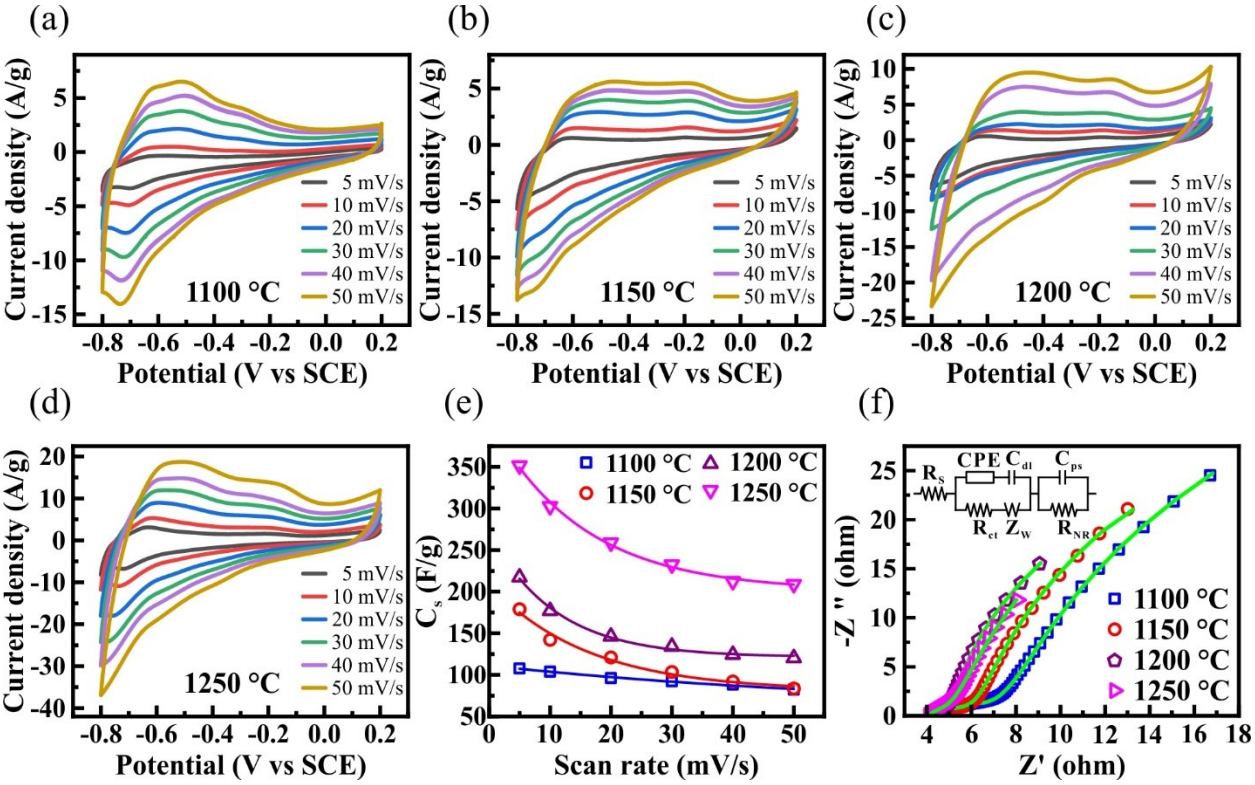

Figure S12. Electrochemical performances. (a)-(d) Cyclic voltammetry (CV) graphs of the Fe_2O_3 nanostructured films@1100, 1150, 1200, and 1250 °C at scan rate of 5, 10, 20, 30, 40, and 50 mV/s in the 1M KOH electrolyte. (e) Specific capacitance values of the Fe_2O_3 nanostructured films are calculated using the CV curves. (f) Nyquist plots for the Fe_2O_3 nanostructured films@1100, 1150, 1200, and 1250 °C. Inset shows a Randles equivalent electrical circuit. All fitting parameters of R_s, CPE, C_{dl}, R_{ct}, Z_W, C_{ps}, and R_{NR} are displayed in Table S2

The electrochemical charge storing properties of Fe_2O_3 nanostructured films@1100, 1150, 1200, 1250 °C are performed via cyclic voltammetry (CV) and electrochemical impedance (EI) spectroscopy in the 1M KOH electrolyte. CV has been successfully used to investigate the capacitive behavior of a material. From the CV results, the specific capacitance (C_s) of the Fe_2O_3 nanostructured films is calculated using equation (2).

$$C_s = \frac{1}{2ms\Delta V} \times \int i.dV \tag{2}$$

where C_s is the specific capacitance (F/g) of the devices, m is the total mass of the 1D nanorods and thin films of Fe_2O_3 nanostructured films deposited on an ITO/glass substrates (g), s is the scan

rate (V/s), ΔV is the potential range, and $\int i.dV$ is an integrated area enclosed within the CV curve. The CV results and the specific capacitances (C_s) at various scan rates of 5, 10, 20, 30, 40, and 50 mV/s are shown in Fig. S12a-e. It is observed that the specific capacitance of the devices decreases as the scan rate increases. The reduction in specific capacitance at high scan rates imputed to the significant barrier for the exchange of electrons on surfaces of the nanorods. The 1D nanorods produced at 1100 ^oC shows lowest specific capacitance value of ~82 F/g at a scan rate of the 50 mV/s whereas, those produced at 1250 ^oC shows highest specific capacitance of ~352 F/g at a low scan rate 5 mV/s. These specific capacitance values are higher than that of Fe_2O_3 thin film,[1] Fe_2O_3 nanorods,[1,2] Fe_2O_3 nanosheets,[2] Fe_2O_3 nanoparticles,[2] nanoporous Fe_2O_3/CNT.[3] This result makes Fe_2O_3 film nanofibers a potential candidate for supercapacitor electrode materials. The capacitance of the various Fe_2O_3 nanostructured films is associated with the resistive constituents, which is studied using electrochemical impedance spectroscopy. The Nyquist plots of the various Fe_2O_3 nanostructured films within limited frequency range are displayed in Fig. S12f. These results are examined through an equivalent circuit model as shown in the inset to Fig. S12f. Using EC-Lab program, all EI spectra are well approximated to the equivalent circuit correlated to the real state of the devices. Note that the definitions of R_s, CPE, C_{dl}, R_{ct}, Z_W, C_{ps}, and R_{NR} are mentioned elsewhere.[4,5] The results of the fitting are displayed in Table S2. At high frequencies, the intercept of impedance arc at the real axis (Z') is the total electrical series resistance (R_s), which is a combination of electrolyte resistance, contact resistance at the interface of active material and the current collector. From the fitting of the data, the R_s values of the Fe_2O_3 nanostructured films found to be approximately the same. The semicircular curved form at high frequencies represents the charge transfer. This semicircle is attributed to the charge transfer resistance (R_{ct}) and constant phase element (CPE). The values of R_{ct} slightly decreased with the elevated synthesis temperatures. R_{ct} is associated with the double layer capacitance (C_{dl}) due to the electric double layer (EDL) mechanism. The C_{dl} values increase with the elevated synthesis temperatures. At a low frequency, the mass transfer comes to control the diffusion behaviors. The Warburg impedance (Z_W) and diffusion resistance (R_{NR}) decrease with the elevated synthesis temperatures. R_{NR} is associated with pseudocapacitance (C_{ps}) of the Fe_2O_3 nanostructured films. The values of C_{ps} increase with the elevated synthesis temperatures. The decrease of the R_{ct}, Z_W, R_{ND} or the increase of the C_{dl} and C_{ps} with the elevated synthesis temperatures indicate the impact of Fe^{2+} cations and cubic (γ) phase on the electrochemical performance of the Fe_2O_3 nanostructured films.

Table S1. The binding energy, FWHM, the peak area, and the concentration of Fe^{2+} cations in the Fe_2O_3 nanostructured films@1100, 1150, 1200, and 1250 ºC.

Temperature (°C)		**1100**	**1150**	**1200**	**1250**
Fe^{2+} $2p_{3/2}$	BE (eV)	710.42	710.2	710.16	709.67
	FWHM (eV)	0.9	1.04	1.03	0.93
	Peak area (eV•count)	1030.39	1710.5	2221.05	2481.71
Fe^{2+} $2p_{1/2}$	BE (eV)	723.60	723.45	723.37	722.9
	FWHM (eV)	1.23	1.17	1.85	1.6
	Peak area (eV•count)	658.95	953.33	2014.05	1981.69
Fe^{3+} $2p_{3/2}$	BE (eV)	711.14	711.03	711.04	710.57
	FWHM (eV)	2.53	2.49	2.76	2.44
	Peak area (eV•count)	16611.41	20889.31	26618.64	19552.6
Fe^{3+} $2p_{1/2}$	BE (eV)	724.86	724.65	724.6	724.14
	FWHM (eV)	2.84	2.78	2.72	2.57
	Peak area (eV•count)	9325.21	11675.45	13086.91	10184.92
Fe^{2+} cations		≈ 6.11%	≈ 7.56 %	≈ 9.63 %	≈ 13.05 %

Table S2. Optimized impedance fitting parameters for the Fe_2O_3 nanostructured films related to the equivalent circuit in Figure S11.

	R_e (Ω)	R_{ct} (Ω)	R_{NR} (Ω)	C_{dl} (F)	C_{ps} (F)	CPE ($F \cdot s^{a-1}$)	a	Z_W ($\Omega\ s^{-1/2}$)
1100 °C	4.41	2.44	77.01	0.055	24.84×10^{-4}	3.68×10^{-4}	0.8043	19.85
1150 °C	4.34	1.65	76.84	0.067	26.71×10^{-4}	10.97×10^{-4}	0.7674	10.82
1200 °C	4.26	0.77	76.31	0.074	31.29×10^{-4}	12.52×10^{-4}	0.8952	6.562
1250 °C	4.14	0.71	70.44	0.083	38.75×10^{-4}	3.37×10^{-4}	0.8969	5.85

Note that R_s represents the total electrical series resistance which is a combination of the electrolyte resistance and contact resistance at the interface between the nanostructured films and electrodes. CPE embodies the constant phase element and is the capacitive impedance related to the double layer capacitance (C_{dl}). R_{ct} represents the charge transfer resistance. Z_W symbolizes the Warburg impedance that is the diffusive impedance associated with the capacitance (C_{dl}) and the charge transfer resistance (R_{ct}). R_{NR} signifies the diffusion resistance on the nanostructured films, which is associated with the pseudocapacitance (C_{ps}).

References

1. Y. Li, J. Xu, T. Feng, Q. Yao, J. Xie and H. Xia, *Adv. Funct. Mater.*, 2017, **27**, 1606728.
2. Y. Li, Q. Li, L. Cao, X. Cui, Y. Yang, P. Xiao and Y. Zhang, *Electrochim. Acta*, 2015, **178**, 171-178.
3. C.-H. Xu, P.-Y. Shen, Y.-F. Chiu, P.-W. Yeh, C.-C. Chen, L.-C. Chen, C.-C. Hsu, I. C. Cheng and J.-Z. Chen, *J. Alloys Compd.*, 2016, **676**, 469-473.
4. M. E. Orazem, I. Frateur, B. Tribollet, V. Vivier, S. Marcelin, N. Pébère, A. L. Bunge, E. A. White, D. P. Riemer and M. Musiani, *J. Electrochem. Soc.*, 2013, **160**, C215-C225.
5. D. V. Pham, R. A. Patil, C.-C. Yang, W.-C. Yeh, Y. Liou and Y.-R. Ma, *Nano Energy*, 2018, **47**, 105-114.